

Semi-implicit scheme for modelling the fluid dynamics part of a DC-powered arc.

Gabriel Barreau[†], *François Pechereau*², *Benjamin Khier*¹, *Philippe Lalande*¹, *Guillaume Puigt*⁴, *Julien Vanharen*³,
*Frédéric Alauzet*³

¹*Université Paris-Saclay, ONERA, DPHY, F-91123 Palaiseau ;*

²*GammaO, Equipe Inria/Onera, Université Paris-Saclay, ONERA, DPHY, F-91123 Palaiseau ;*

³*GammaO, Equipe Inria/Onera, Centre Inria de Saclay, Université Paris-Saclay F-91120 Palaiseau-France ;*

⁴*GammaO, Equipe Inria/Onera, ONERA/DMPE, Université de Toulouse F-31055 Toulouse-France*

gabriel.barreau@onera.fr

[†] Corresponding Author

Abstract

When an aircraft is struck by lightning, the current injected can vary between 200A up to 200kA. The lightning strike can be broken down into two phases. In the pulsed phase, the current intensity can go to 200kA in a few microseconds with compressible flow characteristics, and in the continuous phase, the current is constant with intensities of a few 100A and for durations of hundreds of milliseconds with incompressible flow characteristics. The numerical modelling of this phenomenon is very complex as it involves different physics (fluid dynamics, electromagnetism, radiation ...), and the computational time consumption in the case of 3D simulation is extremely high because the refinement required results in a mesh containing up to several hundred million cells. An ideal solution to reduce this calculation cost would be to mesh only where necessary and, therefore, to have a mesh that will adapt in space and time according to the physics encountered. The magnetohydrodynamic (MHD) 2D/3D code Taranis developed at ONERA is coupled with *feflo.a* [22], an anisotropic mesh adaptation code developed at INRIA. These tools make it possible to greatly reduce the number of nodes in the mesh and, therefore, greatly reduce modelling times. However, as Taranis is a code using explicit compressible methods, the simulation of continuous arcs, even with these mesh adaptation tools, remains very costly due to the incompressible nature of the flow, where very small-time steps must be used to maintain stability. A proposed solution for simulating continuous arcs with a compressible method is to use semi-implicit schemes. The nature of these schemes makes it possible to increase the value of the time steps to values close to those used in incompressible methods while maintaining stability. In this paper, the method of Boscheri et al. [8][9] dealing with the Navier-Stokes equations in real gas is used. Modifications are made to the treatment of real gas, where thermodynamic tables are used instead of equations of state. The scheme is then tested in compressible flow configurations and then in a flow representing, in a simplified way, the flow of a continuous arc. Initial results have shown the scheme's ability to simulate compressible and incompressible flows for larger time steps and with greater accuracy than a conventional compressible scheme.

1. Introduction

In the context of aviation safety, aircraft lightning strikes are studied to understand the direct and indirect damage that this phenomenon can cause when lightning interacts with them [1]. The phenomenon of lightning strikes consists of an electric arc that attaches to the aircraft structure triggering thermal, mechanical and electromagnetic potentially-hazardous responses. The arc is typically characterized by a first short but intense pulsed current followed by a less intense and much longer direct current, which may be superposed by pulsed arcs (return strokes) [2]. The physics of these two types of arc regimes are different since the flow of an arc driven by a pulsed current is highly compressible, whereas that of an arc driven by a direct current is rather incompressible. The Saturne code developed at EDF was used in [3-4] to carry out simulations of continuous arcs. As the Saturne code is based on an incompressible fluid solver, physical limitations appeared when simulating highly compressible fluid associated with pulsed arcs. This led to the ongoing development at ONERA of the massively parallel, finite-volume, three-dimensional magnetohydrodynamics (MHD) code TARANIS, intending to model a full lightning strike. Compressible fluid equations in TARANIS are currently solved temporally using fully explicit methods. These methods are suitable for the highly compressible flows present in pulsed arcs, but the almost incompressible nature of DC-powered arcs means that are less suitable in these regimes, due to the size of the time steps used, which are very small to respect the CFL stability condition. To model the arc evolution during a full lightning strike, we need a numerical

scheme capable of solving flows over a broad range of Mach numbers. Semi-implicit methods seem to meet these conditions. There are many different methods in the literature, but most of them involve solving an implicit pressure equation and then correcting the conservative variables ($\rho u, \rho E$) with this pressure. For the moment, we're focusing on the simulation of a continuous arc using compressible methods. In the literature, many methods use semi-implicit schemes, some of which only deal with Euler equations [5-7], others solve the Navier-Stokes equations for real gases with explicit viscous effects [9-11], for perfect gases with implicit viscous effects [8] or multiphase problems [12]. This paper aims to present a semi-implicit method capable of solving the Navier-Stokes equations where the fluid considered is a real gas, and the viscous and thermal effects are solved implicitly. The present paper is organized as follows: the solved equations are first presented, then we detail the numerical method, and finally, numerical results are shown where first compressible flow test cases are studied, followed by the flow of a hot column representing the flow of a continuous arc.

2. Governing equation

The compressible Navier Stokes equations, i.e., the continuity, momentum and energy equations, are considered. These equations form a set of partially differentiable hyperbolic (PDE) equations written as:

$$\frac{\partial}{\partial t} \begin{pmatrix} \rho \\ \rho \mathbf{u} \\ \rho E \end{pmatrix} + \nabla \cdot \begin{pmatrix} \rho \mathbf{u} \\ \rho \mathbf{u} \otimes \mathbf{u} + p \mathbb{I} \\ \mathbf{u}(\rho E + p) \end{pmatrix} = \nabla \cdot \begin{pmatrix} 0 \\ \boldsymbol{\sigma} \\ \boldsymbol{\sigma} \mathbf{u} + \lambda \nabla T \end{pmatrix} \quad (1)$$

With ρ the fluid density, \mathbf{u} the velocity vector, p the pressure and ρE the total energy density. T is the fluid temperature, λ is the thermal conductivity coefficient, and $\boldsymbol{\sigma}$ is the viscous stress tensor.

To close the system, perfect gas equations of state (EOS) are used if a perfect gas is considered. If a real gas is being considered, EOS are defined using tabulated data.

These tables are generated using an ONERA code called Sethi. Thermodynamical quantities of arbitrary mixtures are evaluated from partition functions assuming local thermodynamic equilibrium and perfect gas law. Energy levels for neutral and ionized atoms are taken from the NIST database [21]. Particle interactions are somewhat introduced in the model as partition functions and are truncated using the minimum value between the Fermi and Griem cutoff [15]. Plasma composition at a given pressure and temperature is obtained by minimization of the mixture Gibbs free energy. Transport coefficients are computed according to the Chapman-Enskog theory [16] with quantities depending on the binary collision integrals and corresponding interaction potentials. Analytical expressions for collision integrals with Debye-screened coulomb potential are used for charged-charged interactions [17]. Neutral-neutral and neutral-charged collision integrals are evaluated using tabulated fits from [18]. For the present work, numerical results for real gases in the following sections have been obtained for an argon gas composed of Ar, Ar⁺, Ar²⁺, Ar³⁺ and electrons. Both thermodynamical and transport quantities have been compared to available data from [20] and show good agreement over temperatures ranging from 300 K to 30000 K and pressures from 1 bar to 100 bar.

The tables used in this code for processing real gases are the pressure-temperature (P, T) and pressure-density (P, ρ) tables. By indicating the two thermodynamic quantities as inputs, the table can give us the value of another thermodynamic quantity (density, temperature, pressure, etc.) or transport quantity (viscosity, thermal diffusion coefficient, etc.). Furthermore, these tables can consider fluid ionization, which is an important parameter to consider given the high temperatures encountered during arc simulation.

The left-hand side of the equation system (1) corresponds to the non-viscous compressible Euler equations, while the right-hand side corresponds to the viscous effects: viscous forces $\boldsymbol{\sigma} \mathbf{u}$ and heat flux $\lambda \nabla T$.

With the Stokes hypothesis, the viscous stress tensor is defined by [19]:

$$\boldsymbol{\sigma} = \mu(\nabla \mathbf{u} + \nabla \mathbf{u}^t) - \frac{2}{3}(\mu \nabla \cdot \mathbf{u}) \mathbb{I} \quad (2)$$

With μ , the dynamic viscosity.

μ and λ are calculated using Sutherland's law (3) in the case of a perfect gas:

$$\mu = \mu_{Su} \left(\frac{T}{T_{Su}} \right)^{\frac{3}{2}} \cdot \frac{T_{Su} + Su}{T + Su}; \quad \lambda = \lambda_{Su} \left(\frac{T}{T_{Su}} \right) \cdot \frac{T_{Su} + Su}{T + Su} \quad (3)$$

Where T_{Su} is a reference temperature equal to 273,15°K, Su a numerical constant which depends on the considerate gas, $\mu_{Su} = \mu(T_{Su})$ and $\lambda_{Su} = \lambda(T_{Su})$. For a real gas, μ and λ can be found by reading the thermodynamic tables.

Let's introduce a split of the energy flow as described in [13]:

$$\mathbf{u}(\rho E + p) = \frac{1}{2} \rho \mathbf{u}^3 + \rho h \mathbf{u} \quad (4)$$

with the specific enthalpy $h = e + \frac{p}{\rho}$. This flow decomposition will enable the construction of an implicit pressure equation, which will be detailed in part 3.

3. Numerical scheme

The numerical scheme is time-discretized using a first-order method. Spatial discretization is also of order 1, using a finite-volume method. The starting point for this method is described in published work by Boscheri et al. [8][9]. In article [9], the Navier-Stokes equations are solved using a semi-implicit pressure method. The scheme covers both perfect and real gases. Real gases are treated using the Redlich-Kwong equations of state and Newton methods. Viscous effects are treated as explicit source terms, while thermal effects can be implicit if the gas is considered perfect. The implicit pressure equation is obtained by splitting the flow of the energy equation into a kinetic energy part and an internal energy part and then injecting the momentum equation into it. In article [8], the method is very similar to that of article [9], but only perfect gases are considered. In this method, viscous effects are implicit with the help of an implicit intermediate velocity equation.

The method described here is based on [8-9], but modifications will be made for the case of real gas processing. Here equations of state are assumed to be provided by tabulated properties. First-order time discretization yields:

$$\frac{\rho^{n+1} - \rho^n}{\Delta t} + \nabla \cdot (\rho \mathbf{u})^n = 0 \quad (5)$$

$$\frac{(\rho \mathbf{u})^{n+1} - (\rho \mathbf{u})^n}{\Delta t} + \nabla \cdot (\rho \mathbf{u} \otimes \mathbf{u})^n + \nabla p^{n+1} = \nabla \cdot \boldsymbol{\sigma}^{n+1} \quad (6)$$

$$\frac{(\rho e)^{n+1} + \frac{(\rho \mathbf{u})^n}{2\rho^n} (\rho \mathbf{u})^{n+1} - (\rho E)^n}{\Delta t} + \nabla \cdot \left(\frac{1}{2} \rho \mathbf{u}^3 \right)^n + \nabla \cdot (h^n (\rho \mathbf{u})^{n+1}) = \nabla \cdot (\boldsymbol{\sigma}^{n+1} \mathbf{u}^{n+1}) + \nabla \cdot (\lambda \nabla T^{n+1}) \quad (7)$$

With conventional explicit compressible schemes, the time step is calculated using formulas (8):

$$\Delta t_{fluid-a} = CFL \min \left(\frac{\Delta x}{|\mathbf{u}| + a} \right); \quad \Delta t_{visc} = CFL \min \left(\frac{\Delta x^2}{2\nu} \right); \quad \Delta t_{th} = CFL \min \left(\frac{\Delta x^2}{\frac{2\lambda}{\rho C_p}} \right) \quad (8)$$

Where a is the sound velocity, ν is the kinematic viscosity, C_p is the heat capacity, and CFL is the Courant-Friedrichs-Lewy condition. By impliciting viscous and pressure terms, viscous and thermal time steps no longer need to be calculated, and the acoustic component of the fluid time step is removed. The effective time step for each iteration then becomes:

$$\Delta t_{fluid} = CFL \min \left(\frac{\Delta x}{|\mathbf{u}|} \right) \quad (9)$$

Spatial discretization is performed using a 1st-order finite-volume method, the mesh used is a cartesian mesh with a space step defined as: $\Delta x = (x_{max} - x_{min})/N$, N being the number of cells in the mesh.

The algorithm solving the system of equations (5-7) consists of five steps:

1. Explicit resolution of the continuity equation (5), which gives the density value at time (ρ^{n+1}). For simplicity of writing, the following notation is used [9]. Let m_i^* be the explicit operator that applies to a generic quantity m_i^n :

$$m_i^* = m_i^n - \frac{\Delta t}{\Delta x} (f_{i+1/2}^m - f_{i-1/2}^m) \quad (10)$$

Here, $f_{i+1/2}^m$ denote the numerical fluxes that are explicitly given by a Rusanov-type approximate Riemann solver:

$$f_{i+1/2}^m = \frac{1}{2} (f(m_{i+1}^n) + f(m_i^n)) - \frac{1}{2} \max(|u_{i+1}^n|, |u_i^n|) (m_{i+1}^n - m_i^n)$$

$$f_{i-1/2}^m = \frac{1}{2} (f(m_i^n) + f(m_{i-1}^n)) - \frac{1}{2} \max(|u_i^n|, |u_{i-1}^n|) (m_i^n - m_{i-1}^n)$$

Where $f(\cdot)$ represents the physical flux related to the variable m . Therefore, using relationship (10):

$$\rho_i^{n+1} = (\rho_i^n)^* \quad (11)$$

2. In the momentum and energy equation, viscous terms are implicit. To construct the implicit pressure equation, the momentum equation is inserted into the energy equation. In so doing, the implicit viscous terms will form a highly non-linear equation since they depend on the velocity gradient. It is then necessary to determine the value of the viscous terms before solving the implicit pressure equation. Taking the approach used in [8], the resolution of a provisional velocity field $\tilde{\mathbf{u}}^{n+1}$ is calculated by solving the following linear system:

$$\rho_i^{n+1} \tilde{\mathbf{u}}_i^{n+1} - \nabla \cdot \boldsymbol{\sigma}^{n+1} = (\rho \mathbf{u})^* - \Delta t \nabla p^n \quad (12)$$

Where $\boldsymbol{\sigma}^{n+1} = \boldsymbol{\sigma}(\tilde{\mathbf{u}}^{n+1})$ according to (2). The linear system is solved using a Thomas algorithm. Once the provisional velocity $\tilde{\mathbf{u}}^{n+1}$ is known, the viscous stress tensor $\boldsymbol{\sigma}^{n+1}$ is calculated using equation (2). In this way, the terms $(\nabla \cdot \boldsymbol{\sigma}^{n+1})$ and $(\nabla \cdot (\boldsymbol{\sigma}^{n+1} \mathbf{u}^{n+1}))$ of equations (6-7) are now known.

3. Inserting the momentum equation into the energy equation gives the following implicit pressure equation:

$$\begin{aligned} & (\rho e)^{n+1} - \frac{\Delta t}{2} \frac{(\rho \mathbf{u})^n}{\rho^n} \nabla p^{n+1} - \Delta t^2 \nabla \cdot (h^n \nabla p^{n+1}) \\ &= (\rho E)^* - \Delta t \nabla \cdot (h^n (\rho \mathbf{u})^*) - \frac{1}{2} \frac{(\rho \mathbf{u})^n}{\rho^n} (\rho \mathbf{u})^* + \Delta t \nabla \cdot (\lambda \nabla T^{n+1}) \end{aligned} \quad (13)$$

Where:

$$(\rho \mathbf{u})^* = (\rho \mathbf{u})^n - \Delta t \nabla \cdot (\rho \mathbf{u} \otimes \mathbf{u})^n + \Delta t \nabla \cdot \boldsymbol{\sigma}^{n+1} \quad (14)$$

$$(\rho E)^* = (\rho E)^n - \Delta t \nabla \cdot \left(\frac{1}{2} \rho \mathbf{u}^3 \right)^n + \Delta t \nabla \cdot (\boldsymbol{\sigma}^{n+1} \mathbf{u}^{n+1}) \quad (15)$$

With $\boldsymbol{\sigma}^{n+1}$ and \mathbf{u}^{n+1} have been calculated in step 2. To solve this equation in pressure, we need to find a way of expressing the remaining implicit terms $((\rho e)^{n+1}, T^{n+1})$ as a function of pressure. Two methods are possible, depending on whether the gas is considered perfect or real.

If the perfect gas is considered: Using the equations of state for perfect gases makes the transformation very simple:

$$(\rho e)^{n+1} = \frac{p^{n+1}}{(\gamma - 1)}; \quad T^{n+1} = \frac{p^{n+1}}{\rho^{n+1} R} \quad (16)$$

With $\gamma = c_p/c_v$ is the ratio of specific heats of the gas, and R is the gas constant. In these conditions, equation (13) becomes:

$$\frac{p^{n+1}}{(\gamma - 1)} - \frac{\Delta t (\rho \mathbf{u})^n}{2 \rho^n} \nabla p^{n+1} - \Delta t^2 \nabla \cdot (h^n \nabla p^{n+1}) - \Delta t \nabla \cdot \left(\lambda \nabla \left(\frac{p^{n+1}}{\rho^{n+1} R} \right) \right) = RHS \quad (17)$$

Where:

$$RHS = (\rho E)^* - \Delta t \nabla \cdot (h^n (\rho \mathbf{u})^*) - \frac{1}{2} \frac{(\rho \mathbf{u})^n}{\rho^n} (\rho \mathbf{u})^* \quad (18)$$

The term ρ^{n+1} is known as it has been calculated in step 1.

If the real gas is considered: In this case, not being able to use the equations of state for perfect gases will make solving the equation more complex. However, the use of thermodynamic tables can simplify this task. The first objective is to be able to express internal energy as a function of pressure at time p^{n+1} .

Using Taylor expansion:

$$(\rho e)^{n+1} \approx (\rho e)^n + \left(\frac{\partial(\rho e)}{\partial p} \right)^n (p^{n+1} - p^n) \quad (19)$$

Where $(\rho e)^n$ and p^n are known, the derivative of internal energy with respect to pressure is calculated beforehand and is available as a thermodynamic value in the tables used. The temperature is also read with the thermodynamic table. As this resolution is only an approximation, an iterative loop is constructed to converge on the result at time p^{n+1} .

This iterative loop is constructed as follows:

- a. Start of the iterative time loop in k , where $m^{k=0} = m^n$. Read the table to know at time t^k all the necessary variables.
- b. Solving the equation:

$$\left(\frac{\partial(\rho e)}{\partial p} \right)^k p^{k+1} - \frac{\Delta t (\rho \mathbf{u})^k}{2 \rho^k} \nabla p^{k+1} - \Delta t \nabla \cdot (h^k \nabla p^{k+1}) = RHS \quad (20)$$

With : $RHS = (\rho E)^* - \Delta t \nabla \cdot (h^k (\rho \mathbf{u})^*) - \frac{1}{2} \frac{(\rho \mathbf{u})^k}{\rho^k} (\rho \mathbf{u})^* - (\rho e)^k + \left(\frac{\partial(\rho e)}{\partial p} \right)^k p^k + \Delta t \nabla \cdot (k \nabla T^k)$

- c. A test on the convergence of the relative error in pressure and temperature is being conducted. The iterative procedure stops when the relative error $\delta = 10^{-8}$ has been reached. Then $p^{n+1} = p^{k+1}$.
4. The pressure p^{n+1} is used to compute the momentum: $(\rho \mathbf{u})^{n+1} = (\rho \mathbf{u})^* - \frac{1}{2} \Delta t \nabla p^{n+1}$
 5. The total energy is computed: $(\rho E)^{n+1} = \rho^{n+1} e^{n+1} + \frac{(\rho \mathbf{u})^n}{\rho^n} (\rho \mathbf{u})^{n+1}$, where the internal energy is computed at the aid of the equation of state if a perfect gas is considered, at the aid of a thermodynamic table if a real gas is considered.

A little remark on the enthalpy used in equations (17) and (20): to compute this enthalpy, equation (21) is used.

$$h_i^n = \frac{\rho_i^n h_i^n}{\rho_i^{n+1}} \quad (21)$$

4. Numerical results

To validate the semi-implicit numerical scheme under compressible flow conditions, a set of simulations of Riemann problems for compressible Euler equations are carried out. These problems consist of two states, left (L) and right (R), separated by a membrane located at $x = x_a$. The computational domain is of size $\Omega = [x_{min}, x_{max}]$ where Neumann-type boundary conditions are imposed at the edges of the domain. Initialization data are

summarized in **Table 1**. It is important to note that all calculations are made assuming that the gas is Argon including compressible test cases. Simulations of these compressible test cases are carried out with schemes that solve Euler's equations in a perfect gas. The numerical scheme presented here will be referred to as SI (semi-implicit). For each test case, the semi-implicit scheme will be compared with an HLL explicit compressible method [14], which is a classical compressible method, and a theoretical curve obtained with an exact Riemann solver for Euler equations. To be in the same conditions as the semi-implicit method, the HLL scheme is of order 1. For all test cases, the mesh is composed of $N=1000$ points, the SI time step is calculated with: $\Delta t = CFL \frac{\Delta x}{|u|}$, the HLL time step with :

$$\Delta t = CFL \frac{\Delta x}{|u|+a}, \text{ with } CFL = 0.5, \text{ } u \text{ the velocity of the flow and } a \text{ the sound velocity.}$$

Name	t_f	x_{min}	x_{max}	x_d	ρ_L	u_L	p_L	ρ_R	u_R	p_R
Fixed contact	2	0.0	1.0	0.5	1.4	0.0	1.0	1.0	0.0	1.0
Moving contact	2	0.0	1.0	0.5	1.4	0.1	1.0	1.0	0.1	1.0
Sod	0.2	0.0	1.0	0.5	1.0	0.0	1.0	0.125	0.0	0.1
Lax	0.14	0.0	1.0	0.5	0.445	0.698	3.528	0.5	0.0	0.571

Table 1 Data of initialization of shock tube problems.

4.1 Fixed and moving contact discontinuity.

Simulation results for a fixed contact discontinuity are shown in Figure 1. It can be observed that both HLL and semi-implicit methods were able to accurately preserve velocity and pressure in the computational domain. However, the behavior of the schemes is not the same in the case of density for the case of a fixed discontinuity (Figure 1).

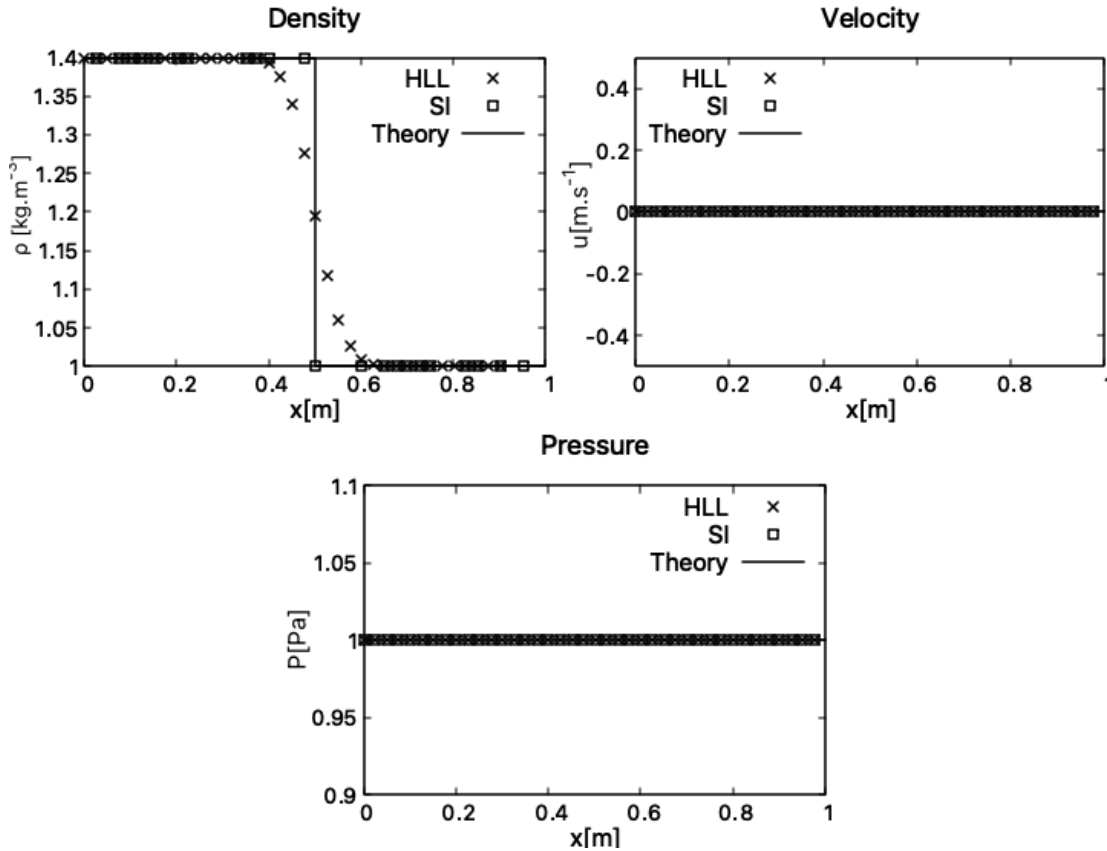


Figure 1: Fixed contact discontinuity at final time $t=2$. Comparison of density, velocity and pressure from the computed solution (symbols) versus the reference solution (straight line)

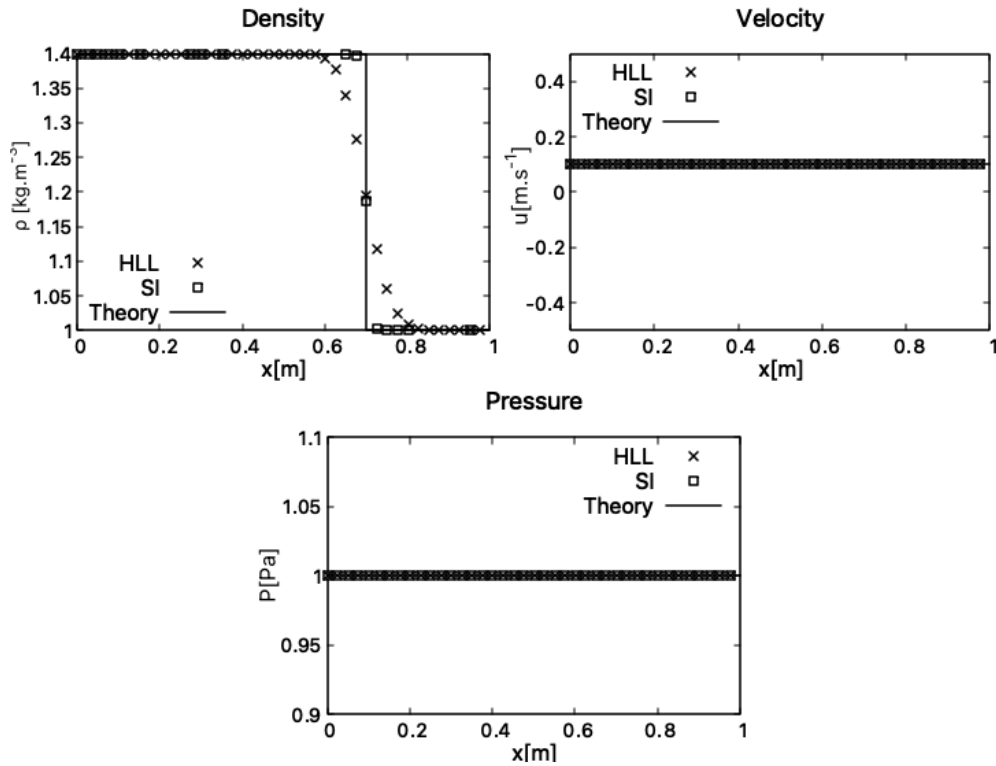


Figure 2: Moving contact discontinuity at final time $t=2$. Comparison of density, velocity and pressure from the computed solution (symbols) versus the reference solution (straight line)

The semi-implicit scheme was able to preserve density in the domain, even though discontinuity, while the HLL scheme diffused it.

In the case of a moving discontinuity (Figure 2), the SI scheme has slightly diffused the density, but the scheme remains less diffusive than the HLL scheme.

Figure 3 shows the value of the time steps as a function of time in the case of a moving discontinuity. Due to the nature of the definition of the time steps used, the SI scheme is able, in this situation, to use time step values which are more than ten times higher compared with the HLL case. This allows the SI scheme to have shorter simulation times than the HLL scheme.

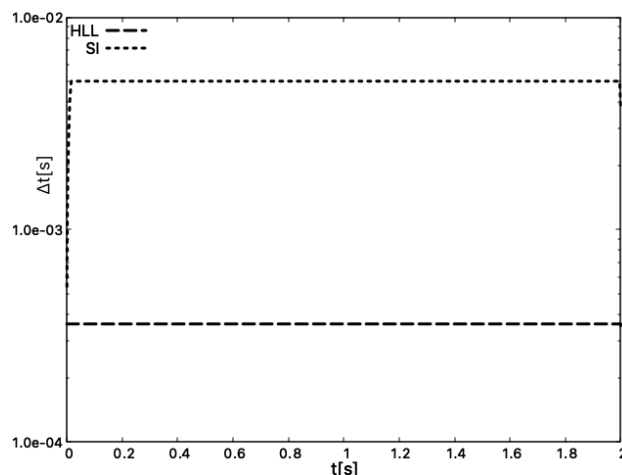


Figure 3 Time step values of HLL scheme and SI scheme for the case of a moving contact discontinuity for $N = 1000$.

4.2 Sod shock tube.

Figure 4 shows the simulation results for the Sod shock tube test case. This is a classic test case used to validate compressible numerical schemes. The problem is characterized by a shock wave propagating through an initially steady-state fluid. This test case is used to assess the ability of a numerical scheme to solve complex phenomena such as shock waves, rarefaction waves and discontinuities. The two numerical schemes simulated the various discontinuities in this flow, notably rarefaction waves and shock waves. Figure 5 plots the value of time steps as a function of time and shows that the time step values of the semi-implicit scheme are larger than those of the HLL method, since they are more than twice as large.

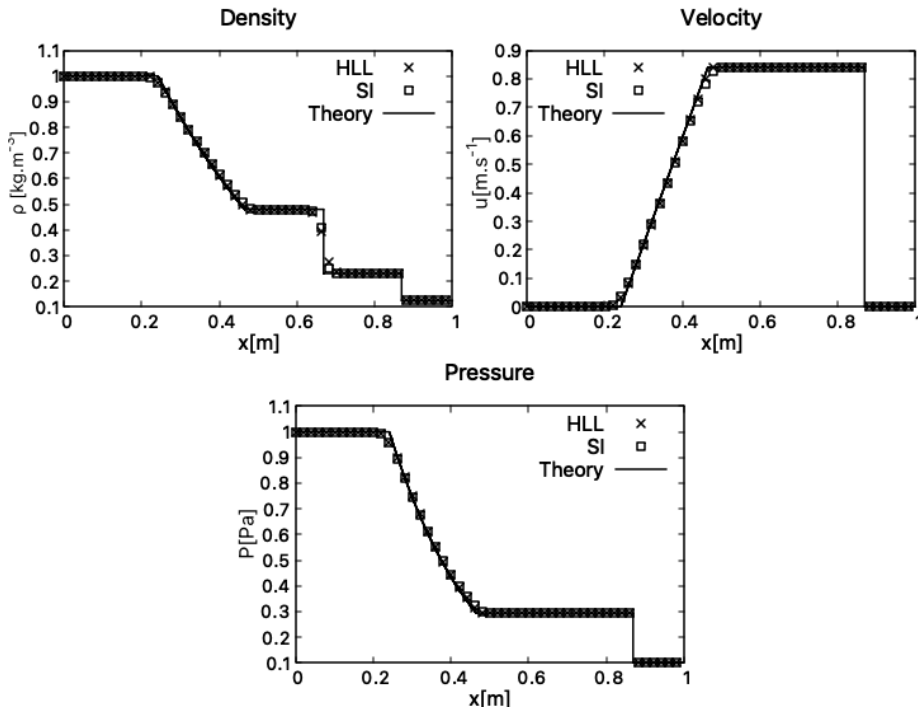


Figure 4: Sod shock tube at final time $t=0.2$. Comparison of density, velocity and pressure from the computed solution (symbols) versus the reference solution (straight line)

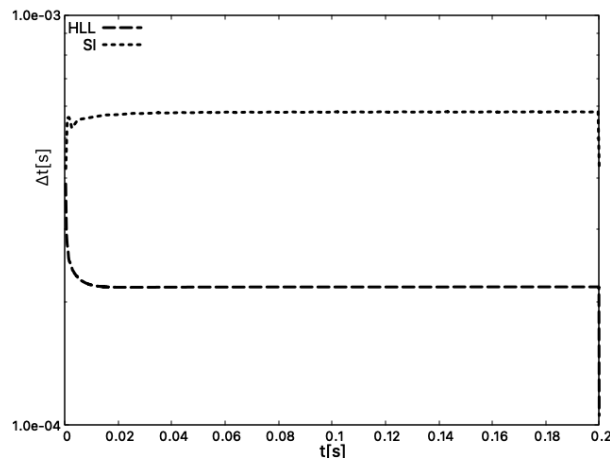


Figure 5 Time step values of HLL scheme and SI scheme for the case of sod shock tube for $N = 1000$.

4.3 Lax shock tube.

This last test case is like that of Sod, but the presence of a velocity discontinuity will make the problem more difficult to solve. Figure 6 shows the result of the simulation. Both schemes give good results, but it is important to notice the presence of a peak value at the shock wave level for the semi-implicit scheme, which can be observed in

all three quantities (density, velocity, pressure). Such peaks also appeared for other semi-implicit schemes such as those presented in [7], [12]. Figure 7 plots the value of time steps as a function of time and shows the same behaviour than the previous test cases where the time step is larger in the case of the semi-implicit method than the explicit compressible method.

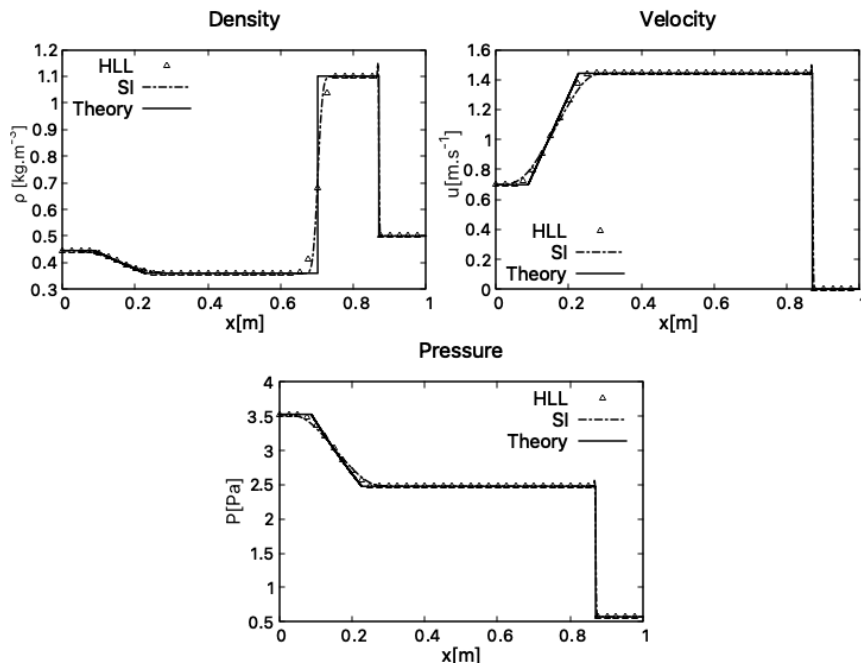


Figure 6 Lax shock tube at final time $t=0.14$. Comparison of density, velocity and pressure from the computed solution (symbols) versus the reference solution (straight line)

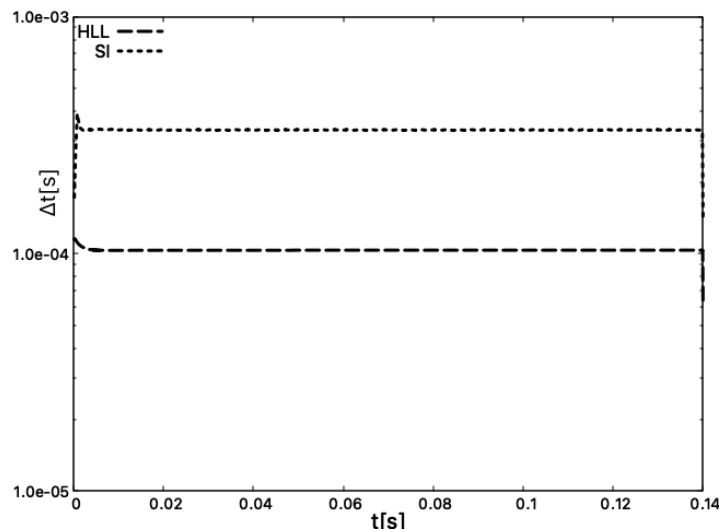


Figure 7 Time step values of HLL scheme and SI scheme for the case of Lax shock tube for $N = 1000$.

To conclude this section, it has been shown that the SI scheme can simulate compressible flows with less numerical diffusion and with larger time steps than a classic compressible scheme: HLL.

4.4 Hot column.

After demonstrating the scheme's ability to simulate compressible flows, it's now time to study its behaviour when faced with DC-powered arc flows. It's important to remember that this new scheme is being studied in a context where the use of compressible schemes is not ideal for continuous arc simulation. The almost incompressible

characteristics of DC-powered arcs mean that simulating this type of arc with a compressible scheme will be extremely time-consuming due to the very small-time steps involved. From a theoretical point of view, the use of the implicit scheme should solve this problem since the acoustic component in the time step calculation is eliminated. A simplified continuous arc can be represented by a hot column advected into the domain. The following section will demonstrate the benefits of the semi-implicit scheme for continuous arc simulation.

As a first step, studying the mesh convergence of the different methods is interesting. A simulation of a 1000°K hot column advected into a 300°K domain will be studied in 3 different configurations: one with the HLL method, one with the perfect gas SI method and finally, one with the real gas SI method.

For each case, the viscosity and thermal effects will not be considered to avoid diffusion effects and CFL = 0.5 for the calculation of the time step. The domain is initiated with constant pressure = 1 bar and constant velocity = 10 m/s. The final time is $t = 0.02s$.

Figure 8 shows mesh convergence for three schemes: a) HLL, b) SI-PG and c) SI-RG.

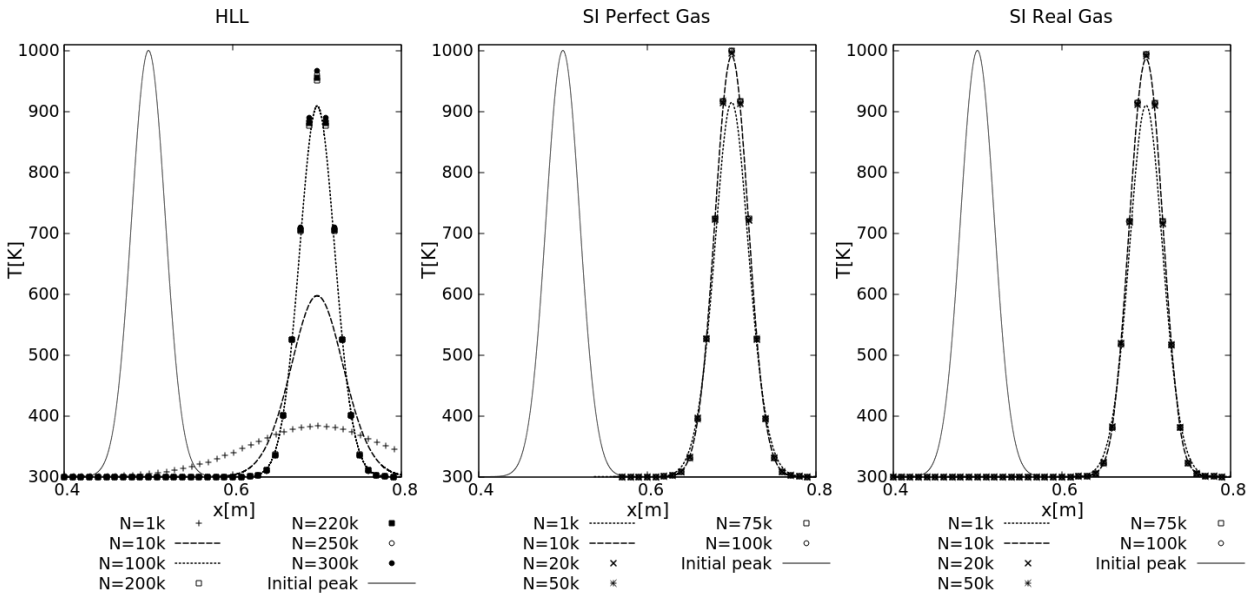


Figure 8 Mesh convergence study of a hot column advected for $t=0.02s$, simulated by a HLL method (left), SI with perfect gas (middle) and SI with real gas (right).

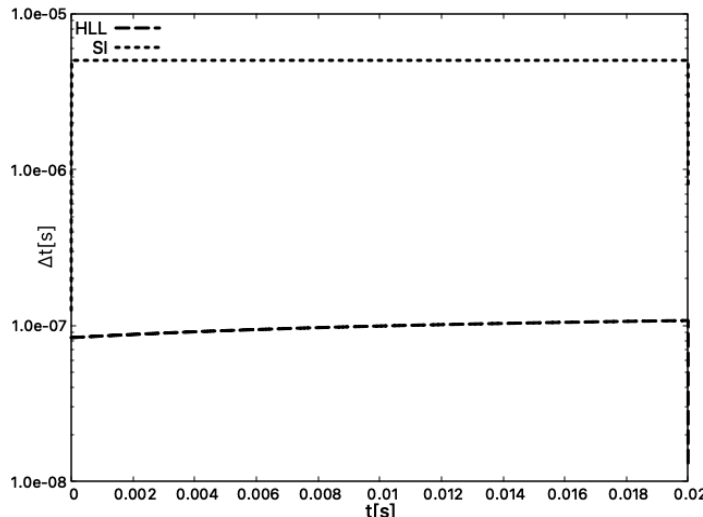


Figure 9 Time step values for the three methods for the case of an advected hot column for $N = 10\,000$.

Due to the highly diffusive nature of the 1st-order HLL scheme, it can be observed that the HLL scheme has difficulty converging, with more than 200k points required to reach the beginning of convergence. On the other hand, even if the semi-implicit schemes are also of order 1, convergence occurs much more quickly at 20k points. Furthermore, to support the fact that the SI scheme is more suitable for simulating a hot column than the HLL scheme, in Figure 9, the value of time steps as a function of time is plotted. The SI time step value is approximately 2

orders of magnitude larger than that of the HLL scheme. The semi-implicit scheme then enables less time-consuming simulations with much less diffusive behaviour.

4.5 Viscous and thermal effects.

In this section, the effects of viscosity and temperature are studied, and two points are analyzed:

- Their influence on the shape of curves compared to the case where they are neglected.
- Their influence on the calculation of the time step.

Figure 10 shows the temperature trends in two configurations: on the left, a hot column with a maximum value of 1000K is advected for $t = 0.02s$; on the right, the same test case but with a column with a maximum value of 9000K. As was shown in the previous section, this test case is converged on a 20,000-point mesh; these two flows will be simulated on this same mesh. Figure 11 shows this convergence of the temperature curves with the viscous effects for the perfect gas case. Figure 10 shows: the peak at initialization (line), the advected peak in a case where viscous and thermal effects are not considered (dash line), a peak with a perfect gas method with viscosity and thermal effects, and a real gas method with viscosity and thermal effects (symbols). As seen in the previous section, on a converged mesh, the viscosity-free case has, in both cases, not diffused, and the temperature peak has the same value as that of the initialization. This is because no diffusive terms are considered in solving the equations.

However, in cases where viscosity is considered, different behaviour is observed in both cases. For the 1000k case (left in Figure 10), both the real gas and perfect gas curves have diffused, but only by a small amount and have very similar values: a maximum temperature value of 990K for the perfect gas case and 985K for the real gas case. It is important to remember that the viscous and thermal coefficients in the perfect gas case are calculated using Sutherland's law (3). This law is valid up to temperature values of around 2500K. To conclude this case, the thermal and viscous effects are quite weak.

However, for the 9000K column, different behaviour is observed. In this case, the fluid is much hotter, so the thermal effects are much greater. These greater thermal effects are at the origin of the greater diffusion of the curves corresponding to the schemes that take these thermal and viscous effects into account. We also note a difference in values between the real gas and perfect gas cases: the peak temperature for the real gas is 7545K, while the perfect gas case is 7467K. This difference can be explained by the fact that at 9000K, Sutherland's law (3) used in the perfect gas case is no longer valid. One of the parameters that explains why this equation is no longer valid is the ionization effects that occur at such temperatures, which are not considered, unlike in the tables given by the Sethi code. These ionization effects will, among other things, modify the chemical composition of the gas and thus alter the behaviour of transport coefficients (viscosity, diffusion coefficient...).

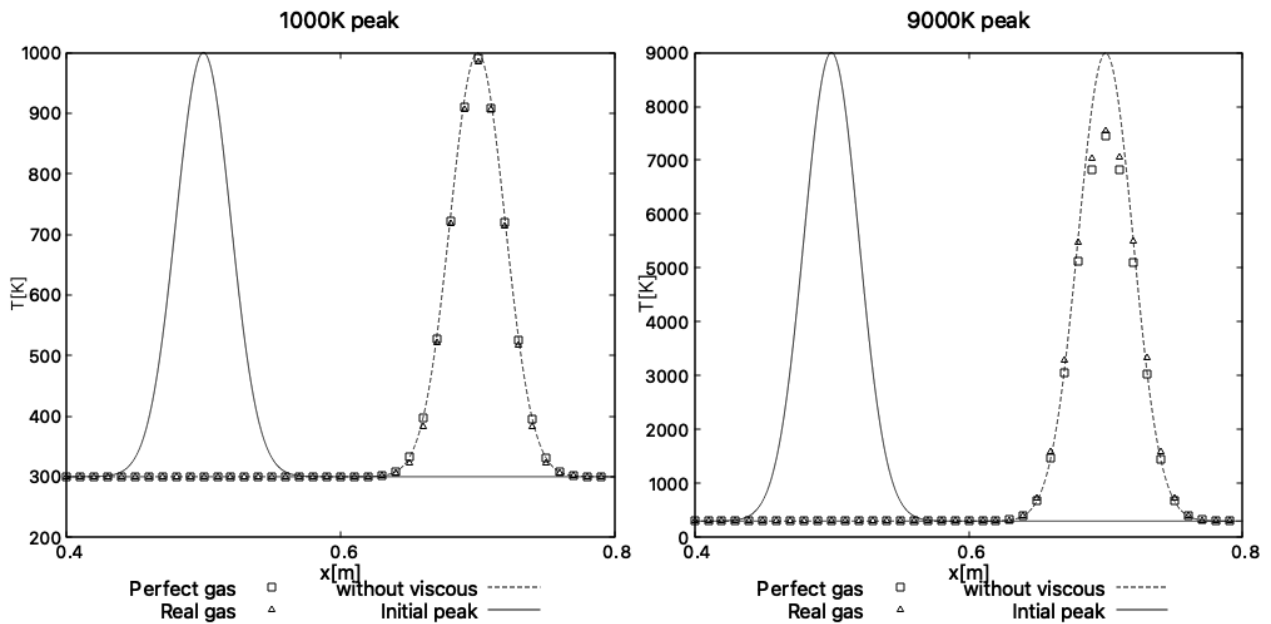


Figure 10: Influence of viscous and thermal effects for a hot column at 1000K (left) and 9000K (right).

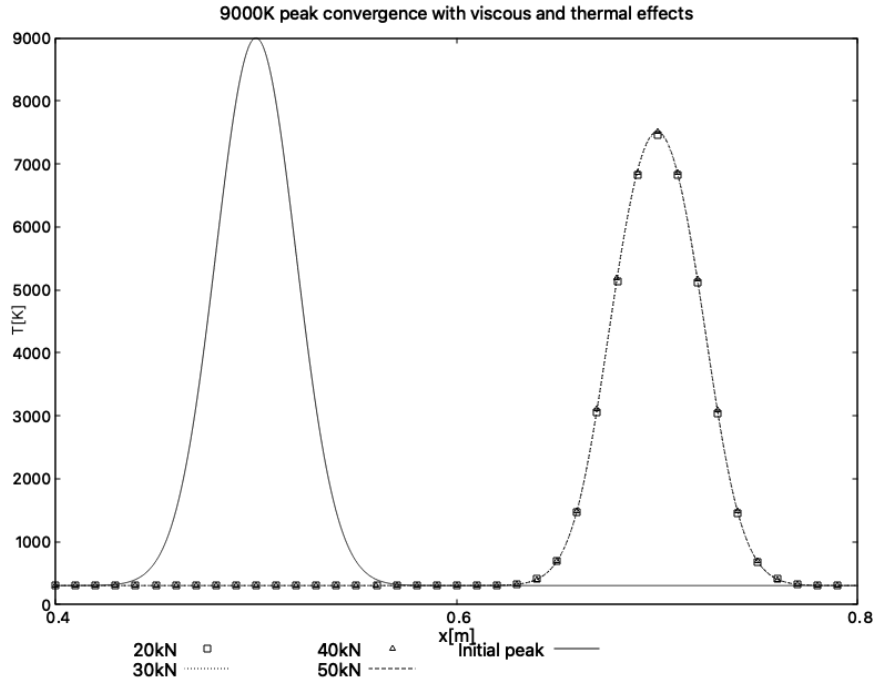


Figure 11: Temperature convergence for the case of a 9000K hot column advected for 0.02s.

How will the addition of viscous and thermal effects influence the calculation of the time step? It was shown in the previous section that if the fluid Euler equations are solved alone, the time steps used are at least two orders of magnitude larger than those of a classical explicit compressible scheme. However, if the Navier Stokes equations (1) are solved, the time step is calculated using the equations (8). To summarize, at each time iteration, the three-time steps (8) are calculated, and the smallest of the three is chosen as the effective time step. In the semi-implicit scheme shown, as viscous and thermal effects are implicit, these time steps are not considered, and only the time step (9) is calculated. However, stability problems were observed during simulations with a high temperature peak (over 5000K) on a highly refined mesh (over 20,000 points). After empirical investigation, the following point was observed:

Even if the thermal time step is not calculated, our effective time step must not be too far from it. To explain this phenomenon, the case of hot columns at 1000K and 9000K presented above is considered. For both cases, the ratio between the effective time step calculated with (9) and the time steps calculated with (8) are calculated where for all times step $CFL = 0.5$. The results are summarized in **Table 2**.

	$\frac{\Delta t_{fluid}}{\Delta t_{th}}$	$\frac{\Delta t_{fluid}}{\Delta t_{fluid-a}}$	$\frac{\Delta t_{fluid}}{\Delta t_{visc}}$
1000°K	1.16	62	2
9000°K	125	178	17

Table 2: Ratio between the effective time step and those of the explicit compressible diagrams for the case of a hot column at 1000K and a column at 9000K with a $CFL = 0.5$ and $N = 20\ 000$ for all calculations.

Under these conditions, calculating the column at 1000K gives good results, whereas calculating the column at 9000K gives oscillations. This difference in behavior may be correlated with the fact that the difference in value between the effective time step and the explicit compressible time steps is much greater in the 9000K case. In fact, according to **Table 2**, in the case of 1000K, the fluid time step and the thermal time step are almost equal, whereas in the case of 9000K, the fluid time step is more than 100 times greater (with a $CFL = 0.5$). In this test case, where thermal effects are important, having too great a difference in value between

time steps makes the computation unstable. The temperature curves at 9000K plotted in Figure 10 were obtained with the following CFL values: $CFL = 0.1$ for the perfect gas case, and $CFL = 0.05$ for the real gas case. The new ratios of time steps in these conditions are summarized in Table 3 where $CFL = 0.5$ for the other time steps (8).

	$\frac{\Delta t_{fluid}}{\Delta t_{th}}$	$\frac{\Delta t_{fluid}}{\Delta t_{fluid-a}}$	$\frac{\Delta t_{fluid}}{\Delta t_{visc}}$
9000°K(PG)	11	64	5
9000°K(RG)	11	17	2

Table 3 Ratio between the effective time step and those of the explicit compressible diagrams for the case of a hot column at 1000K and for a column at 9000K with a $CFL=0.1$ for Δt_{fluid} and $N=20\ 000$ for all calculation.

So, even if the CFL had to be reduced to obtain a condition where the scheme is stable, the ratio between the effective time step and those used with an explicit compressible method remains significant (approximately an order of magnitude). Given the initial results, for this type of flow, having a $\frac{\Delta t_{fluid}}{\Delta t_{th}} \leq 11$ is a prerequisite for a stable simulation. It is important to note that this criterion is currently purely empirical, valid only for this flow and that studies are underway to determine a true stability criterion valid for all types of flow. It's important to note that the effects of viscosity have not been discussed simply because, in this flow, the velocity is constant throughout the domain, so its effect is negligible.

5. Conclusion

In this article, a semi-implicit scheme has been presented. This scheme aims to be able to simulate compressible flows as well as weakly compressible flows where the fluid considered is a real gas. The various test cases simulated with this scheme have demonstrated the code's ability to simulate compressible flows with good accuracy and shorter computation times than with a conventional compressible scheme. In the second part, the code's ability to simulate flows of the type that can be encountered when simulating a DC-powered arc was carried out. It was seen that the scheme was much less diffusive and converged much faster than a conventional compressible scheme and that the simulation time was much faster due to the time steps being about two orders of magnitude larger in the case where viscous and thermal effects are neglected and one order of magnitude when viscous are thermal effects are considered. Finally, it has been shown that the use of thermodynamic tables for the treatment of real gases will give results in better agreement with physics since at the temperatures encountered, ionization effects appear, which are not considered with classical equations of state. However, to validate this hypothesis, a comparison between the results of the literature and those of the simulations will have to be carried out in the future. It has been determined that particular attention needs to be paid to the time step values when simulating viscous/thermal effects. The prospects of this work are to include this scheme in a 2D/3D configuration in the Taranis MHD code, which will significantly improve computation times when simulating continuous arcs with this code.

5. References

- [1] : Martins, R. S. (2016). *Experimental and theoretical studies of lightning arcs and their interaction with aeronautical materials* (Doctoral dissertation, Universite Paris-Saclay).
- [2]: Lalande, P., & Delannoy, A. (2012). Numerical methods for zoning computation. *Aerospace Lab*, (5), p-1.
- [3] : Tholin, L., Chemartin, P., & Lalande, F. (2013, September). Numerical investigation of the surface effects on the dwell time during the sweeping of lightning arcs. In *2013 International Conference on Lightning and Static Electricity (ICOLSE 2013)*.
- [4] : Archambeau, F., Méchitoua, N., & Sakiz, M. (2004). Code Saturne: A finite volume code for the computation of turbulent incompressible flows-Industrial applications. *International Journal on Finite Volumes*, 1
- [5] : Patnaik, G., Guirguis, R. H., Boris, J. P., & Oran, E. S. (1987). A barely implicit correction for flux-corrected transport. *Journal of Computational Physics*, 71(1), 1-20.

- [6] : Moguen, Y., & Dick, E. (2020). Diffusion and dissipation in acoustic propagation simulation by convection-pressure split algorithms in all Mach number form. *Journal of Computational Physics*, 414, 109480.
- [7] : Kwatra, N., Su, J., Grétarsson, J. T., & Fedkiw, R. (2009). A method for avoiding the acoustic time step restriction in compressible flow. *Journal of Computational Physics*, 228(11), 4146-4161.
- [8]: Boscheri, W., & Tavelli, M. (2022). High order semi-implicit schemes for viscous compressible flows in 3D. *Applied Mathematics and Computation*, 434, 127457.
- [9]: Boscheri, W., & Pareschi, L. (2021). High order pressure-based semi-implicit IMEX schemes for the 3D Navier-Stokes equations at all Mach numbers. *Journal of Computational Physics*, 434, 110206.
- [10]: Denner, F., Evrard, F., & van Wachem, B. G. (2020). Conservative finite-volume framework and pressure-based algorithm for flows of incompressible, ideal-gas and real-gas fluids at all speeds. *Journal of Computational Physics*, 409, 109348.
- [11] : Cordier, F., Degond, P., & Kumbaro, A. (2012). An asymptotic-preserving all-speed scheme for the Euler and Navier–Stokes equations. *Journal of Computational Physics*, 231(17), 5685-5704.
- [12] : Jemison, M., Sussman, M., & Arienti, M. (2014). Compressible, multiphase semi-implicit method with moment of fluid interface representation. *Journal of Computational Physics*, 279, 182-217.
- [13] : Toro, E. F., & Vázquez-Cendón, M. E. (2012). Flux splitting schemes for the Euler equations. *Computers & Fluids*, 70, 1-12.
- [14] : Toro, E. F., & Toro, E. F. (2009). The HLL and HLLC Riemann solvers. *Riemann Solvers and Numerical Methods for Fluid Dynamics: A Practical Introduction*, 315-344.
- [15] : Colonna, G.; Laricchiuta, A. Thermodynamic and Transport Properties of Equilibrium Debye Plasmas. *Entropy* **2020**, 22, 237.
- [16]: Hirschfelder, J. O., Curtiss, C. F., & Bird, R. B. (1964). Molecular theory of gases and liquids. *Molecular theory of gases and liquids*.
- [17] : Hahn, H. S., Mason, E. A., & Smith, F. J. (1971). Quantum transport cross sections for ionized gases. *The Physics of Fluids*, 14(2), 278-287.
- [18] : Bruno, D., Capitelli, M., Catalfamo, C., Celiberto, R., Colonna, G., Diomede, P., ... & Pirani, F. (2008). Transport properties of high-temperature Mars-atmosphere components. *ESA Scientific Technical Review*, 256.
- [19] : White, F. M., & Majdalani, J. (2006). *Viscous fluid flow* (Vol. 3, pp. 433-434). New York: McGraw-Hill.
- [20] : Murphy, A. B., & Tam, E. (2014). Thermodynamic properties and transport coefficients of arc lamp plasmas: argon, krypton and xenon. *Journal of Physics D: Applied Physics*, 47(29), 295202.
- [21]: P.J. Linstrom and W.G. Mallard, Eds., NIST Chemistry WebBook, NIST Standard Reference Database Number 69, National Institute of Standards and Technology, Gaithersburg MD, 20899
- [22]: Alauzet, F., & Frazza, L. (2021). Feature-based and goal-oriented anisotropic mesh adaptation for RANS applications in aeronautics and aerospace. *Journal of Computational Physics*, 439, 110340.